

# Electronic excitations in atomic clusters: beyond dipole plasmon

V.O. Nesterenko<sup>1</sup>, P.-G. Reinhard<sup>2</sup>, and W. Kleinig<sup>1,3</sup>

<sup>1</sup> *Bogoliubov Laboratory of Theoretical Physics,*

*Joint Institute for Nuclear Research,*

*Dubna, Moscow region, 141980, Russia*

<sup>2</sup> *Institut für Theoretische Physik II,*

*Universität Erlangen, D-91058, Erlangen, Germany and*

<sup>3</sup> *Technische Universität Dresden, Inst. für Analysis, D-01062, Dresden, Germany*

(Dated: September 6, 2018)

## Abstract

Multipole electron modes beyond the Mie plasmon in atomic clusters are investigated within the time-dependent local density approximation theory (TD-LDA). We consider the origin of the modes, their connection with basic cluster properties and possible routes of experimental observation. Particular attention is paid to infrared magnetic orbital modes, scissors and twist, and electric quadrupole mode. The scissors and twist modes determine orbital magnetism of clusters while the electric quadrupole mode provides direct access to the single electron spectra of the cluster. We examine two-photon processes (Raman scattering, stimulated emission pumping and stimulated adiabatic Raman passage) as the most promising tools for experimental investigation of the modes.

## I. INTRODUCTION

Besides the dominant dipole Mie plasmon, many other electron modes, both electric and magnetic, can exist in atomic clusters [1]. These modes are known in diverse many-body systems (atomic nuclei, quantum dots, dilute gas of trapped fermionic and bosonic atoms, etc). It is a demanding problem to observe them in atomic clusters. The multipole electron modes represent an essential part of electron dynamics in both collective and electron-hole domains. They are connected with basic cluster properties and thus can serve as an effective tool for their investigation.

We will pay the main attention to three infrared modes: scissors magnetic dipole (M1), twist magnetic quadrupole (M2) and electric quadrupole (E2). These modes are connected basic properties of atomic clusters. Besides, they are the strongest spin-saturated modes beyond the Mie plasmon.

The scissors and twist modes are of orbital magnetic character [2, 3, 4, 5]. In general, the scissors mode exists only in deformed systems. It dominates the Van Vleck paramagnetism [3, 6] and can result in dia-para magnetic anisotropy in particular light atomic clusters [6]. The twist mode is the strongest magnetic orbital mode in spherical clusters where the scissors mode vanishes [5]. It is mainly generated by transitions between electron levels with maximal orbital moments. Altogether, the scissors and twist modes are fundamental sources of orbital magnetism in spin-saturated clusters. In deformed clusters, the scissors M1 is coupled to electric quadrupole E2 mode.

The infrared E2 mode is most interesting in two particular cases of deformed clusters: free light deformed clusters and embedded oriented rods (strongly prolate large clusters). In the first case, the E2 mode is reduced to a few electron-hole excitations driven by cluster deformation. As was recently demonstrated, these excitations allow to determine the mean field spectra of light clusters [7]. Being sensitive to cluster structure, these spectra can deliver important information on diverse cluster features. And last, but not least, the infrared electron-hole quadrupole excitations have a good chance to be observed in particular two-photon processes.

Infrared E2 modes in oriented silver rods embedded into glass matrices [8, 9] represent another useful example of non-dipole electron motion in clusters. These modes are collective and in principle can be studied in Raman scattering (experiments of this kind are in progress

[10]). Because of the extreme axis ratio, rods represent a unique sample for investigation of both E2 and M1 (scissors) collective motion.

Being non-dipole, the infrared multipole states cannot be populated by one-photon transitions which excite exclusively dipole modes. Thus one has to use two-photon processes (TPP) where the target state is populated via an intermediate dipole state by two (absorption and emission) dipole transitions. The dipole plasmon or isolated dipole states can serve as the intermediate state. Some of the processes, Raman scattering (RS), stimulated emission pumping (SEP), and stimulated adiabatic Raman passage (STIRAP), are widely used in atomic and molecular spectroscopy to populate non-dipole modes but their applications to clusters are still very limited and, at a first glance, even questionable. The problems are caused by particular clusters properties (dense spectra, broad level structures, harmonicity of collective modes, short lifetimes, non-radiative decay channels, etc) which can hamper TPP. Nevertheless, we will show that TPP listed above can be applied to clusters and deliver valuable information on cluster properties (see preliminary discussion and first estimations in [7]). Specific requirements to TPP applications will be considered in detail.

The manuscript provides a survey of explorations from a theoretical perspective. To that end, we employ the microscopic time-dependent local-density-approximation (TDLDA) theories in the linear regime [11] and beyond it [12, 13]. The main aim of our study is to outline non-dipole electron modes in clusters and encourage their investigation in TPP experiments.

The paper is outlined as follows. In Sec. II, we give a brief overview of infrared multipole modes, clarify their origin and connection with basic cluster features. In Sec. III, the two-photon processes RS, SEP and STIRAP are inspected as possible routes of experimental study of the modes. Mainly free light deformed clusters are considered. A summary is given in Sec. IV.

## II. HIERARCHY OF MULTIPOLE MODES

### A. Classification scheme

Multipole modes are oscillations of multipolarity  $\lambda\mu$  which are typical for finite many-body systems. It is useful to distinguish collective and non-collective multipole modes. In

the first case, one deals with a superposition of many elementary excitations which form a coherent motion while in the second case the mode represents a mixture of only a few elementary excitations. In mesoscopic systems with  $10 - 10^4$  particles, we have an intermediate (and maybe the most complicated) situation when a large number of small elementary components contribute coherently and thus form the collective part of the mode while a few dominant components determine its particle-hole structure. Just such systems will be considered in the present study. More specifically, we will deal with metal clusters where valence electrons move freely in a common mean field. The single-particle levels of the mean field are bunched into quantum shells [14, 15] which constitute a key point in understanding the nature of multipole modes and their classification.

A useful sorting scheme for single-particle levels of valence electrons in metal clusters is provided by the three-dimensional harmonic oscillator [14, 15, 16]. The levels of a spherical cluster are sorted in perfectly degenerate bunches (major quantum shells) which are characterized by the principle quantum number  $\mathcal{N} = 0, 1, 2, \dots$ . The shells are separated by appreciable energy gaps and every shell involves only states of the same space parity  $\pi = (-1)^{\mathcal{N}}$ . This oscillator picture is well fulfilled in light clusters and provides still a good approximation in medium and heavy ones. In axially deformed clusters, the single-electron levels are characterized by Nilsson-Clemenger quantum numbers  $\nu = [\mathcal{N}n_z\Lambda]$  where the principle shell number  $\mathcal{N} = n_z + 2n_r + \Lambda$  is expressed through the numbers of nodes in radial ( $n_r$ ) and symmetry axis ( $n_z$ ) directions and projection  $\Lambda$  of the orbital moment onto the symmetry axis [16].

Following this scheme, excitations of valence electrons are characterized by the  $\Delta\mathcal{N}$  value, the difference in shell for the dominant  $1eh$  jumps. Quadrupole excitations have even parity and are collected into the branches  $\Delta\mathcal{N} = 0$  and 2. The excitations with larger  $\Delta\mathcal{N}$  are weak and can be neglected. The branch  $\Delta\mathcal{N} = 0$  has low excitation energy. It exists only in deformed systems (with partly occupied valence shell) and vanishes in spherical systems (with fully occupied valence shell). In the next subsections, we will use this sorting scheme for explanation of the origin and properties of quadrupole E2, scissors M1 and twist M2 modes.

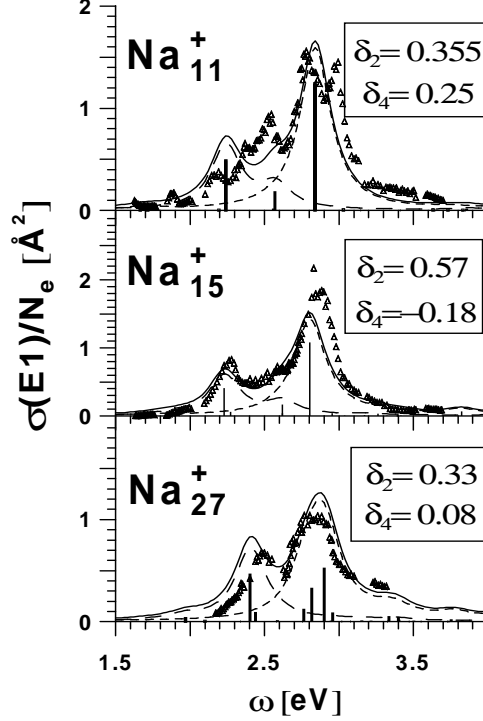


FIG. 1: Photoabsorption dipole cross section in light axially deformed Na clusters. Quadrupole and hexadecapole deformation parameters are indicated in boxes. RPA results are given as vertical bars (in  $\text{eV } \text{\AA}^2$ ) and as a strength function smoothed by the Lorentz weight with the averaging parameter 0.25 eV. Separate contributions to the strength function from the  $\lambda\mu = 10$  and 11 dipole branches (the latter is twice stronger) are shown by dash curves. The experimental data (triangles) from [21] are given for the comparison.

## B. Calculation scheme

The electron cloud is described by density-functional theory at the level of the local-density approximation (LDA) for the ground state and time-dependent LDA (TDLDA) for the excitations, using actually the functional of [17]. The ionic background of the cluster is approximated by the soft jellium model allowing for quadrupole and hexadecapole deformations [13, 18]. In the analysis given in this section, the infrared modes stay in the regime of small amplitudes. We thus employ the linearized TDLDA, often called the random-phase-approximation (RPA). The actual implementation for axially symmetric clusters is explained in [11]. The reliability of the method has been checked in diverse studies of the Mie plasmon in spherical [19] and deformed [11, 20] clusters. As an example, Fig. 1 demonstrates quite

good agreement of our results with the experimental data [21] for the dipole plasmon in light deformed clusters at room temperature.

The proper choice of the light clusters to be studied is very important. i) The clusters should be small enough to possess a dilute and non-collective infrared spectrum. Only then the spectrum can be resolved and unambiguously related to the single-particle levels. ii) Since infrared modes are mainly induced by cluster deformation (see discussion in the next subsection), the clusters with a strong deformation (either prolate or oblate) are desirable. The simplest case of axial shape is most suitable for the analysis. iii) Shape isomers exhibit different single-electron spectra [11, 20, 22], which can smear out the low-energy spectral lines. The heavier clusters, the more isomers [11, 20]. So, light clusters with one dominant equilibrium shape are preferable. Between them, we should choose the clusters whose ground state and first isomers have the similar (prolate or oblate) shape. Thus we will minimize the spectral blurring. iv) The jellium approximation is certainly rough for description of details in light clusters, which establishes a lower limit for the cluster size. The results for the smallest samples may not reach a quantitative level, but they are still useful for the first consideration. As is demonstrated in Fig. 1, even in the lightest clusters the jellium TDLDA sufficiently well reproduces the basic characteristics of the Mie plasmon (average energy, principle gross-structure, magnitude of the deformation splitting of the resonance), see for discussion [7, 20]. Such accuracy suffices for our present survey. For this reason, as well as for the sake of simplicity, our study will exploit the jellium approximation.

### C. Quadrupole mode

We start our analysis with quadrupole excitations in light deformed free sodium clusters. The hierarchy of E2 modes is illustrated in Fig. 2 in terms of normalized quadrupole photoabsorption [11]  $\sigma(\text{E2}, \omega)/N_e \sim \sum_j \langle j | r^2 Y_{2\mu} | 0 \rangle^2 \omega_j^3 \eta(\omega_j - \omega)$  calculated within RPA (here  $\omega_j$  is the energy of RPA  $j$ -state and  $\eta$  is the Lorentz weight function). Though E2 modes are not observed in the photoabsorption, it is instructive for a first overview. Let us first consider the strong quadrupole resonance appearing at high frequencies in the range 2-4 eV. In heavy clusters this resonance is associated with the quadrupole plasmon. The resonance is mainly formed by E2 transitions over two major shells ( $\Delta\mathcal{N} = 2$ ). It exists in clusters of any shape and exhausts most of the quadrupole strength. Though the resonance is

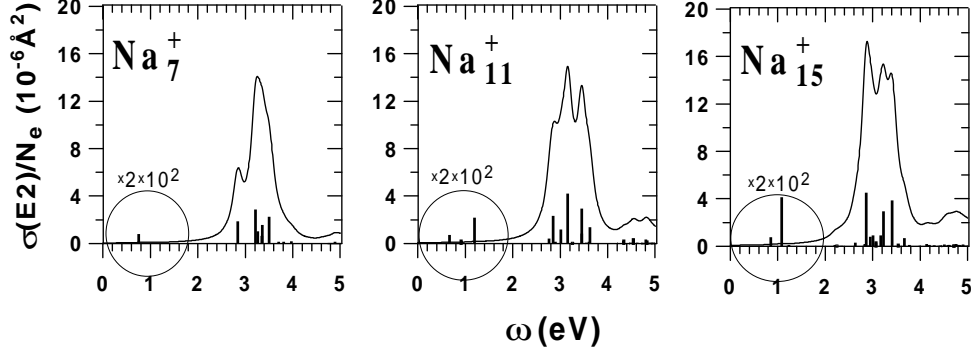


FIG. 2: Quadrupole photoabsorption in light deformed clusters  $\text{Na}_7^+$ ,  $\text{Na}_{11}^+$  and  $\text{Na}_{15}^+$ . The results are given as bars for every discrete state and as smooth strength functions obtained by folding with a Lorentzian of width  $\Delta = 0.25$  eV. The weak infrared part of the strength (enclosed by the circles at 0.5-1.5 eV) is rescaled by the factor  $2 \cdot 10^2$ .

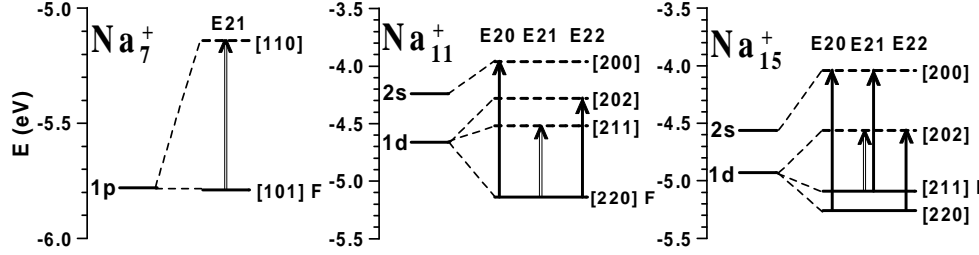


FIG. 3: The electron level schemes for  $\text{Na}_7^+$ ,  $\text{Na}_{11}^+$  and  $\text{Na}_{15}^+$  in the spherical limit (left) and at the equilibrium deformation (right). Occupied and unoccupied single-particle levels are drawn by solid and dash lines, respectively. The Fermi (HOMO) level is marked by index F. Arrows depict the possible low-energy hole-electron  $E2\mu$  transitions. Double arrows represent transitions of the scissor nature between the members of the deformation multiplet.

energetically close to the dipole Mie plasmon, it can be discriminated by means of angular-resolved electron energy-loss spectroscopy (AR-EELS) at electron scattering angles  $\sim 6^\circ$  [23].

In the present study, we are not so much interested in the quadrupole plasmon but in non-collective infrared quadrupole modes which can deliver important information about the electron single-particle spectrum near the Fermi (=HOMO) level. The infrared spectra are associated with the low-energy  $\Delta\mathcal{N} = 0$  branch created by E2 transitions inside the valence shell. Being of the  $\Delta\mathcal{N} = 0$  origin, most of these spectra can exist only in clusters

with *partly* occupied valence shell, i.e. in deformed clusters. The deformation splits the infrared quadrupole mode into branches  $\lambda\mu = 20, 21$  and  $22$ . In Fig. 1, the infrared modes reside at 0.5-1.5 eV. As compared with the quadrupole plasmon, the infrared spectrum is very dilute. It is represented only by a few well separated levels. This prevents mixing of  $1eh$  configurations by the residual interaction and creation of collective states. The infrared quadrupole modes persist to keep their  $1eh$  nature. As is seen from Fig. 1, they have very weak quadrupole strength in the photoabsorption. But they may be accessible in two-photon processes.

Fig. 3 shows single-particle levels and  $E2\mu$ -transitions inside the valence shells in  $\text{Na}_7^+$ ,  $\text{Na}_{11}^+$ , and  $\text{Na}_{15}^+$ . The levels can be characterized by Nilsson-Clemenger quantum numbers [16]  $\nu = [\mathcal{N}n_z\Lambda]$ . The  $1eh$  pairs corresponding to the transitions read  $\{[101] - [110]\}_{21}$  in  $\text{Na}_7^+$ ,  $\{[220] - [200]\}_{20}$ ,  $\{[220] - [211]\}_{21}$ ,  $\{[220] - [202]\}_{22}$  in  $\text{Na}_{11}^+$ , and  $\{[220] - [200]\}_{20}$ ,  $\{[211] - [202]\}_{21}$ ,  $\{[211] - [200]\}_{21}$ ,  $\{[220] - [202]\}_{22}$  in  $\text{Na}_{15}^+$ . Following this scheme, the infrared modes in Fig. 2 can be unambiguously identified as particular  $1eh$  configurations. The modes have different photoabsorption strengths depending on value of their E2-transition matrix element  $\langle 1eh | r^2 Y_{2\mu} | 0 \rangle$ . The RPA calculations which allow in principle any composition of states confirm that the infrared modes are indeed almost pure  $1eh$  states. In every mode the dominant  $1eh$  component typically attains 99 – 100%.

The infrared modes provide valuable information about cluster's properties. As is seen from 3, most of the transitions connect the levels arising due to deformation splitting. The corresponding infrared modes are determined by the deformation and vanish at the spherical shape. Thus they deliver information on the deformation splitting of the electron levels in the HOMO-LUMO region. Besides, being combined with photoemission data for the spectra of occupied electron states (see e.g. [24]), the infrared  $1eh$  modes immediately yield energies of unoccupied electron states. As a result, one can get the complete electron spectrum in the HOMO-LUMO region. This spectrum is sensitive to different cluster features (interplay of equilibrium and isomer cluster's shapes, ionic structure, correlations, temperature effects, etc.) and so can serve as an effective tool for investigation of these features.

Finally, it is worth noting that in deformed systems the electric and magnetic modes with the same projection  $\mu$  and space parity  $\pi$  are mixed. The mixture of electric E21 and magnetic orbital M11 excitations is especially interesting as it provides access to the orbital M1 scissors mode [2, 4, 6]. The properties of this mode are sketched in the next subsection.



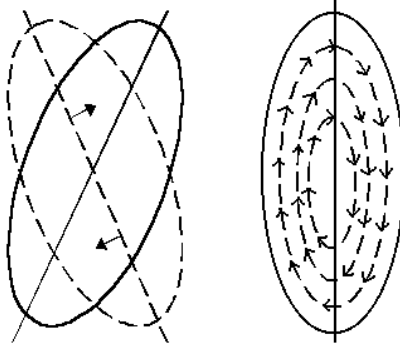


FIG. 4: *Macroscopic view of scissors mode : rigid rotation [25] (left), and rotation within a rigid surface [3] (right).*

#### D. Scissors mode

The scissors mode (SM) is a general collective flow already predicted or found in different finite quantum systems (atomic nuclei [25, 26], quantum dots [27] and ultra-cold superfluid gas of fermionic atoms [28]). Besides, this mode is used as an indicator of Bose-Einstein condensate in the dilute gas of trapped Bose atoms [29, 30]. In atomic clusters, the SM was predicted [2, 4] but, in spite of some attempts [31], not yet observed. Obviously, the SM demonstrates a universal character. It is pertinent to any finite systems with two features in common: broken spherical symmetry (deformation) and a two-component nature. In the systems listed above, these components are neutrons and protons in nuclei, valence electrons and ions in atomic clusters, electrons and surrounding media in quantum dots, atoms and the trap in dilute Fermi and Bose gases. The SM features were recently reviewed in [6].

##### 1. Macroscopic view

The macroscopic collective nature of SM can be illustrated by the geometrical model first proposed for atomic nuclei [25]. For clusters, this model exhibits SM as scissors-like small-amplitude oscillations of valence electrons versus the ions, both assumed to form distinct spheroids (see left part of Fig. 4). Hence the name *scissors* mode. Obviously, such a mode can exist only in deformed systems.

Following the alternative view of [3] (right part of Fig. 4), the displacement field of the

mode is a sum of the rigid small-amplitude rotation and irrotational quadrupole term (the latter provides vanishing velocity of electrons at the surface):

$$\vec{u}(\vec{r}) = \vec{\Omega} \times \vec{r} + \delta_2(1 + \delta_2/3)^{-1} \nabla(yz) \quad (1)$$

where  $\Omega$  is the angular velocity and  $\delta_2 = 3/2 (R_{\parallel}^2 - R_{\perp}^2)/(R_{\parallel}^2 + 2R_{\perp}^2)$  is the parameter of quadrupole deformation expressed via the semi-axes of the ellipsoidal system. Both macroscopic treatments, [3, 25], include the rigid rotation of valence electrons versus the ions with the restoring force originating from the Coulomb interaction between the electrons and ions. But the model [3] has the additional irrotational quadrupole term. Its physical sense becomes clear if we take into account that the SM, like the quadrupole E2 modes, is separated into low-energy ( $\Delta\mathcal{N} = 0$ ) and high-energy ( $\Delta\mathcal{N} = 2$ ) branches. The first rotational term in (1) is responsible for the  $\Delta\mathcal{N} = 0$  branch while the second irrotational term generates the  $\Delta\mathcal{N} = 2$  branch. Thus the branches have quite different physical nature. This feature is exploited as a signature of the Bose-Einstein condensate in dilute gas of trapped Bose atoms [29, 30]. Unlike the normal phase which exhibits both SM branches, the condensate phase supports only the irrotational flow. So, a vanishing  $\Delta\mathcal{N} = 0$  branch serves as a fingerprint of the condensate.

The rotational low-energy branch  $\Delta\mathcal{N} = 0$  corresponds to a large extent to the scissors scenario exhibited in left part of Fig. 4 and thus is usually treated as a true SM. In atomic clusters, just this branch is responsible for van Vleck paramagnetism and other effects of orbital magnetism. In what follows, we will concentrate on this part of SM.

In axial clusters, the low-energy SM is generated by the orbital momentum fields  $L_x$  and  $L_y$  perpendicular to the symmetry axis  $z$ . The mode is represented by the states  $|\Lambda^\pi = 1^+ \rangle$  where  $\Lambda$  is the eigenvalue of  $L_z$  and  $\pi$  is the space parity. Energy and magnetic strength of the mode are estimated as [2, 3, 4, 6]

$$\omega = \frac{20.7}{r_s^2} N_e^{-1/3} \delta_2 \text{ eV}, \quad (2)$$

$$B(M1) = 4 \langle 1^+ | \hat{L}_x | 0 \rangle^2 \mu_b^2 = \frac{2}{3} N_e \overline{r^2} \omega \mu_b^2 \simeq N_e^{4/3} \delta_2 \mu_b^2 \quad (3)$$

where  $N_e$  is the number of valence electrons,  $r_s$  the Wigner-Seitz radius (in  $\text{\AA}$ ), and  $\mu_b$  is the Bohr magneton. We use here atomic units  $m_e = \hbar = c = 1$ . The value  $B(M1)$  stands for summed strength of the degenerated x- and y-branches. The z-branch vanishes for symmetry

reasons. It is worth noting that  $B(M1)$  transition strength does not depend on  $r_s$  and so is the same for different metals. Both energy and magnetic strength are proportional to the deformation parameter  $\delta_2$  and thus vanish in spherical systems. So, the SM exists only in system with a broken spherical symmetry. The larger the deformation, the stronger the low-energy scissors mode.

It is worth noting that we assume here global deformation of the system. At the same time, spherical symmetry can be broken locally while keeping the global spherical shape. This takes place, e.g., in spherical clusters where the ionic background as such destroys locally the spherical symmetry and gives rise to some M1 (though rather weak) orbital strength even with *zero* global deformation [32].

The irrotational  $\Delta\mathcal{N} = 2$  branch of SM takes place in both systems, spherical and deformed. Its energy maps the energy of the quadrupole plasmon. In fact the irrotational SM is a part of this plasmon.

## 2. Microscopic view

The microscopic treatment of the SM is based on the shell structure of axially deformed mean field [4, 6]. The angular momenta orthogonal to the symmetry axis,  $\hat{L}_x$  and  $\hat{L}_y$ , promote low-energy  $\Delta\mathcal{N} = 0$  transitions inside the valence shell and high-energy  $\Delta\mathcal{N} = 2$  transitions across two shells.

It is instructive to expand the wave functions of the single-electron states in terms of the spherical basis ( $nL\Lambda$ )

$$\Psi_{\nu=[\mathcal{N}n_z\Lambda]} = \sum_{nL} a_{nL}^{\nu} R_{nL}(r) Y_{L\Lambda}(\Omega). \quad (4)$$

This allows to evaluate the single-particle orbital M1 transition amplitude between hole ( $\nu = h$ ) and particle ( $\nu = p$ ) states:

$$\langle \Psi_p | \hat{L}_x | \Psi_h \rangle \propto \delta_{\pi_p, \pi_h} \delta_{\Lambda_p, \Lambda_h \pm 1} \sum_{nL} a_{nL}^p a_{nL}^h \sqrt{L(L+1) - \Lambda_h(\Lambda_h \pm 1)}. \quad (5)$$

Eq. (5) shows that the scissors mode is generated by  $\Lambda_p = \Lambda_h \pm 1$  transitions between the components of the same spherical ( $nL$ )-level. In spherical systems ( $nL\Lambda$ )-states belonging to the level ( $nL$ ) are degenerate while in deformed systems they exhibit the deformation splitting and so may be connected by M1 transitions with non-zero excitation energies. This is the microscopic origin of the scissors mode. The energy scale of the scissors mode is

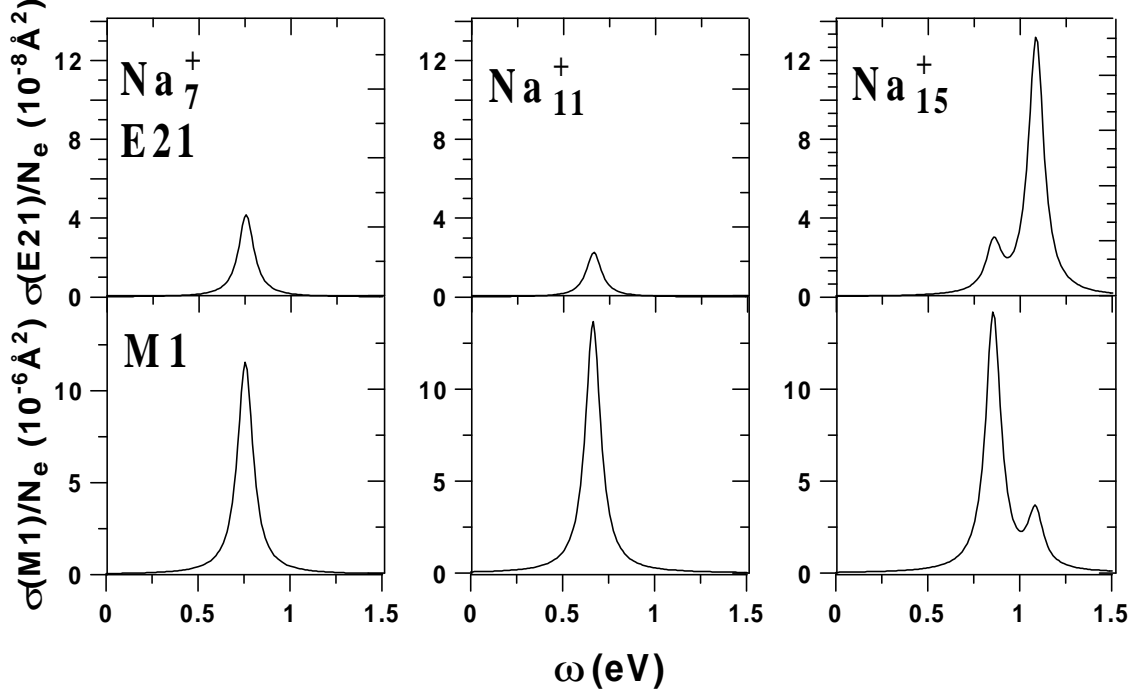


FIG. 5: *E21 and scissors M1 photoabsorption for infrared modes in light deformed clusters.*

determined by the deformation energy splitting and so is rather small. This explains the predominantly low-energy ( $\Delta\mathcal{N}=0$ ) character of the true SM.

There is an intimate connection between the scissors and quadrupole E21 modes in deformed clusters. In fact, both SM and E21 are parts of a general motion characterized by the states  $|\Lambda^\pi = 1^+ \rangle$ . To illustrate this point, let's again consider Eq. (5). As was mentioned above, the SM operator connects only components from one and the same basis level  $nL$ . This is because the operators  $\hat{L}_x$  and  $\hat{L}_y$  have no  $r$ -dependent part and so, due to orthogonality of the radial wave functions  $R_{nL}(r)$ , cannot connect the components with different  $nL$ . But the latter can be done by the quadrupole operator  $r^2 Y_{21}$ . In this sense the SM operator is more selective than E21, though both operators generate transitions of the same multipolarity. The states  $|\Lambda^\pi = 1^+ \rangle$  involve both SM and E21 modes and respond to both M11 and E21 external fields. The states are treated as magnetic or electric, depending on each of the two responses dominates.

The dual nature of the states  $|\Lambda^\pi = 1^+ \rangle$  is demonstrated in Fig. 5. The one-to-one correspondence between the E21 and SM peaks takes place. These peaks represent  $1\hbar$  states  $\{[101] - [110]\}_{21}$  in  $\text{Na}_7^+$ ,  $\{[220] - [211]\}_{21}$  in  $\text{Na}_{11}^+$ , and  $\{[211] - [200]\}_{21}$ ,  $\{[211] - [202]\}_{21}$

in  $\text{Na}_{15}^+$ . The first free states originate from the deformation splitting of spherical levels and thus give rise to SM. In principle, these states carry both E21 and SM flows and the ratio between two contributions depends on the actual state structure. The plot for  $\text{Na}_{15}^+$  gives an instructive example. It is seen that the lower peak determined by  $[211] \rightarrow [202]$  transition between the members of the deformation multiplet exhibits an appreciable magnetic dipole strength and thus should carry a large SM fraction. Just such deformation-induced infrared states provide access to SM. Instead, the higher peak is determined by a  $[211] \rightarrow [200]$  transition which takes place even in spherical case. The deformation is not crucial here. This state favors the E21 field and so can be treated as an ordinary quadrupole mode.

### 3. *Effects of orbital magnetism*

Static orbital magnetism in clusters was widely explored during last decades. The studies were mainly based on the Landau theory of the atomic magnetism [33]. A variety of issues was covered: giant dia- and paramagnetism in weak magnetic fields [34, 35], size and temperature effects [36, 37], manifestation of quantum supershells in magnetic susceptibility [37], influence of cluster shape (both axial and triaxial) on the magnetic properties [3, 38], anisotropy of magnetic susceptibility in deformed clusters [3, 38], orbital magnetism of supported clusters [39], etc..

In the present study, we will consider some principle points of the orbital magnetism, connected with the scissors mode: the decisive role of SM in van Vleck paramagnetism [3, 6] and the related effect of dia-para anisotropy in magnetic susceptibility of particular light clusters [6]. The latter effect displays a peculiarity of small clusters to exhibit strong variations in their properties with a cluster size. For example, RPA calculations [4, 6] show that the SM energies and  $B(M1)$  strengths, though mainly scaling with the deformation  $\delta_2$  and the electron number  $N_e$  according to the trends (2) and (3), demonstrate, nevertheless, strong fluctuations. This can affect the magnetic susceptibility and lead, in particular cases, to dia-para anisotropy.

At this point, we introduce a few equations to make the discussion more precise. The interaction of cluster valence electrons with a uniform magnetic field  $B_k$  applied along the coordinate axis  $k$  is

$$\hat{H}_{int} = \mu_b B_k \hat{L}_k + \frac{1}{2} \mu_b^2 B_k^2 \rho_k^2 \quad (6)$$

where  $k = x, y, z$  is the coordinate index,  $\hat{L}_k = \sum_{a=1}^{N_e} \hat{L}_k^{(a)}$  is the  $k$ -th projection of the angular momentum operator (the sum runs over all valence electrons),  $\rho_z^2 = \sum_{a=1}^{N_e} (x_a^2 + y_a^2)$ ,  $\rho_x^2 = \sum_{a=1}^{N_e} (y_a^2 + z_a^2)$ , and  $\rho_y^2 = \sum_{a=1}^{N_e} (x_a^2 + z_a^2)$ . We neglected in (6) electron spins since for clusters considered below (axial sodium clusters with even  $N_e$  and completely filled Fermi level) their contribution to the magnetic susceptibility is expected to be small.

If the magnetic field is weak, one can use the perturbation theory. Then, up to the second order to  $B_k$ , the induced change of the ground state energy is

$$\begin{aligned} \omega_0^{int} = \mu_b B_k < 0 | \hat{L}_k | 0 > - \mu_b^2 B_k^2 \sum_{j \neq 0} \frac{| < j | \hat{L}_k | 0 > |^2}{\omega_j} \\ + \frac{1}{2} \mu_b^2 B_k^2 N_e \overline{\rho_k^2} \end{aligned} \quad (7)$$

where  $\omega_j$  is the energy of the excited state  $|j >$  and  $\overline{\rho_k^2}$  is the average value of  $\rho_k^2$ . The negative second and positive third terms in (7) are responsible for the temperature independent van Vleck paramagnetism and Langevin diamagnetism, respectively.

The first (linear) term in (7) dominates in the systems with a partly filled Fermi level since in this case there is only incomplete mutual compensation of the contributions of the valence electrons with different orbital projections  $\Lambda$ . In particular, this term results in a strong diamagnetic moments  $\mu = \mu_b |\Lambda|$  in axial clusters with odd  $N_e$  [38]. In magic spherical clusters, where the Fermi level is fully occupied, both the first linear and second quadratic terms are zero and these clusters are again diamagnetic [38]. This diamagnetism is called giant [35] since, due to  $\overline{\rho_k^2} \gg a_0^2$  ( $a_0$  is the Bohr radius), it is much stronger than the atomic one.

We will consider axially (z-symmetric) deformed clusters with even  $N_e$  and fully occupied Fermi level. In this case, the linear term in (7) is zero but there remains the van Vleck term for  $k = x, y$ . The orbital magnetic susceptibility  $\chi_k = -\partial^2 \omega_0^{int} / \partial B_k^2$  is then the sum of Langevin diamagnetic and van Vleck paramagnetic terms:

$$\chi_k = \chi_k^{dia} + \chi_k^{para}, \quad (8)$$

where

$$\chi_k^{dia} = -\mu_b^2 N_e \overline{\rho_k^2} = -\mu_b^2 \Theta_k^R, \quad (9)$$

$$\chi_k^{para} = 2\mu_b^2 \sum_{j \neq 0} \frac{| < j | \hat{L}_k | 0 > |^2}{\omega_j} = \mu_b^2 \Theta_k, \quad (10)$$

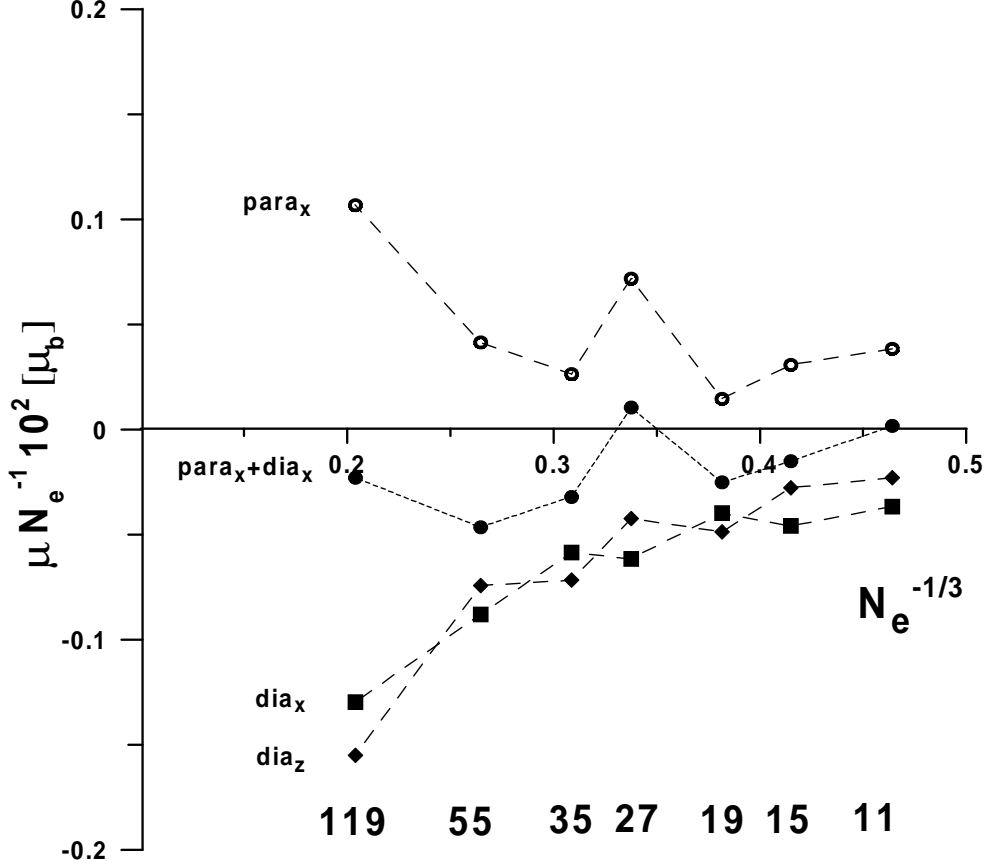


FIG. 6: Normalized diamagnetic, paramagnetic and summed moments  $\mu = \chi B_k$  ( $B_k = 4T$ ) in axial deformed clusters  $\text{Na}_{11}^+$ ,  $\text{Na}_{15}^+$ ,  $\text{Na}_{19}^+$ ,  $\text{Na}_{27}^+$ ,  $\text{Na}_{35}^+$ ,  $\text{Na}_{55}^+$  and  $\text{Na}_{119}^+$ .

having denoted by

$$\Theta_k = 2 \sum_{j \neq 0} \frac{|\langle j | \hat{L}_k | 0 \rangle|^2}{\omega_j} \quad (11)$$

the cranking moment of inertia and by

$$\Theta_k^R = N_e \overline{\rho_k^2} \quad (12)$$

its rigid moment of inertia.

Note that for  $k = x, y$  the operator entering in the matrix element in (10) is exactly the scissors generator. This makes evident that just the *low-energy* SM mainly contributes to  $\chi_{x,y}^{para}$ . Following our calculations [6], this contribution achieves 85 – 100%. So, just *the SM determines the van Vleck paramagnetism*.

In the schematic model [3], the moment of inertia comes out as the rigid-body value, so that  $\theta_{x,y} = \theta_{x,y}^R$  and  $\chi_{x,y}^{para} = -\chi_{x,y}^{dia}$ , i.e. a complete compensation of dia- and paramagnetic

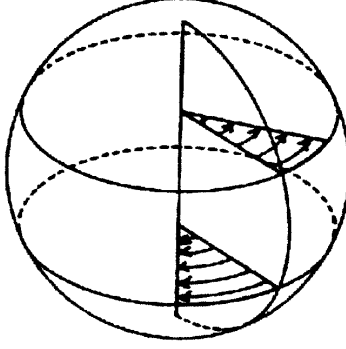


FIG. 7: *Macroscopic image of twist mode.*

terms in  $\chi_{x,y}$  takes place. Due to axial symmetry, one also has  $\chi_z^{para} = 0$ . The total susceptibility becomes, therefore, strictly anisotropic [3]

$$\chi_x = \chi_y = 0, \quad \chi_z = \chi_z^{dia}, \quad (13)$$

varying from zero to diamagnetic values.

However, strong shell effects in some light clusters may alter appreciably the above result. This is illustrated for  $\text{Na}_{27}^+$  in Fig. 6. Because of very low excitation energy of the SM in this cluster [4, 6], the paramagnetic susceptibility is so much enhanced that it cannot be balanced by the diamagnetic term. So,  $\text{Na}_{27}^+$  gains the remarkable property to be paramagnetic in x,y-directions and diamagnetic in z-direction. The cluster  $\text{Na}_{11}^+$  also hints this property. Though dia- and paramagnetism are weak as compared with other forms of magnetism, the dia-para anisotropy described above is big enough to be measured experimentally. This effect is only one of the examples of diverse unusual magnetic properties of small clusters (see [39] for a recent review). Altogether, these properties may provide an interesting perspective for new technologies.

### E. Twist mode

The SM is the dominant orbital magnetic mode in deformed clusters. But in spherical clusters the SM vanishes and the next orbital magnetic mode, twist M2, becomes the strongest one [5].

This twist was first proposed as an quadrupole torsional vibrational flow of an elastic globe [40]. The mode is generated by the operator  $\hat{T} = e^{-i\alpha z L_z} = e^{\alpha \vec{u} \cdot \vec{\nabla}}$  with the velocity field



$\vec{u} = (yz, -xz, 0)$  and small angle  $\alpha$  [40, 41]. The macroscopic image of twist is presented in Fig. 7. The mode is treated as small-amplitude rotation-like oscillations of upper hemisphere against the lower hemisphere. The rotational angle of horizontal layers is proportional to  $z$  (projection to the axis of rotation). So, the flow vanishes at the equator and poles of the system.

The restoring force of the twist is determined by the quadrupole distortions of the Fermi surface in the *momentum* space. So, the twist represents transverse magnetic quadrupole oscillations of an *elastic* medium, generated by variation of the kinetic-energy density. The twist is a general feature of any 3-dimensional finite Fermi system which exhibits an elastic behavior. The twist mode is well known in atomic nuclei and still remains an actual topic of both theoretical and experimental studies [41]-[44]. The interest on twist is motivated by the fact that this mode is a remarkable example of an elastic vortex motion. The twist was also predicted but not yet observed in atomic clusters [5, 43] and trapped dilute gas of Fermi atoms [45].

Unlike the M1 scissor mode which exists only in deformed systems, the twist takes place in Fermi systems of any shape, spherical and deformed. As the magnetic quadrupole mode, the twist is represented by  $|\Lambda^\pi = 2^- \rangle$  states of unnatural space parity. Twist energy and M2 strength in atomic clusters are estimated as [5]

$$\omega = 17eV \mathring{A}^2 r_s^{-2} N_e^{-1/3}, \quad B(M2) = 0.52 r_s^2 N_e^2 \mu_b^2 \quad (14)$$

where  $B(M2)$  is the probability of M2 transition from the ground state to  $2^-$  twist state. It is easy to see that the generating operator of the twist,  $zL_z \propto r(Y_{10}L_z)$ , coincides with the orbital component  $\mu = 0$  of  $M2$  transition operator [46]

$$\hat{F}(M2, \mu) = \mu_b \sqrt{10} r [g_s \{Y_1 \hat{s}\}_{2\mu} + \frac{2}{3} g_l \{Y_1 \hat{L}\}_{2\mu}] \quad (15)$$

which is the sum of spin and orbital contributions with  $g_s = 2$  and  $g_l = 1$ . So, it is natural to consider the twist as a part of the orbital M2 motion.

Let's consider now the microscopic features of the twist. Figure 8 exhibits results of the microscopic calculations [5] for the orbital M2 strength  $B(M2) = |\langle 2^- | \hat{F}(M2) | 0 \rangle|^2$  in light, medium and heavy spherical sodium clusters. Only the orbital part of the M2 transition operator is used. It is seen that the dominant twist strength is concentrated in a single 1eh peak with the lowest energy. This peculiarity persists independent of  $N_e$ , though the degree

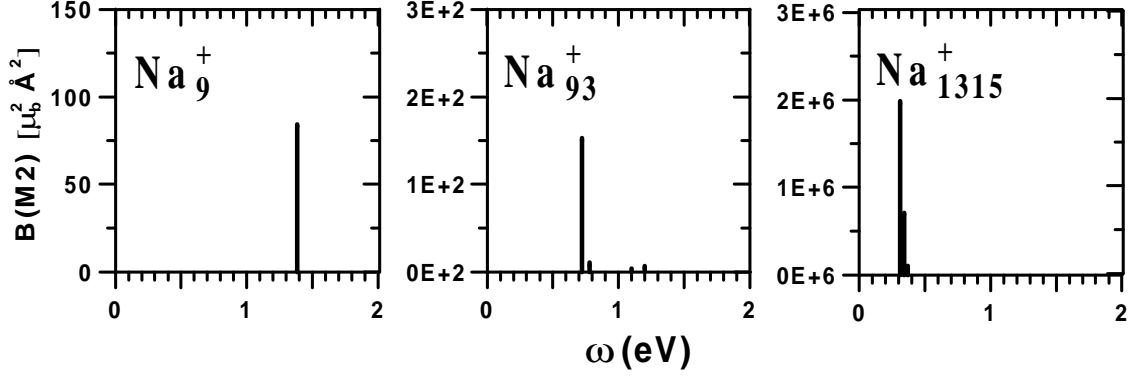


FIG. 8: The distribution of M2-strength in spherical Na clusters of a different size.

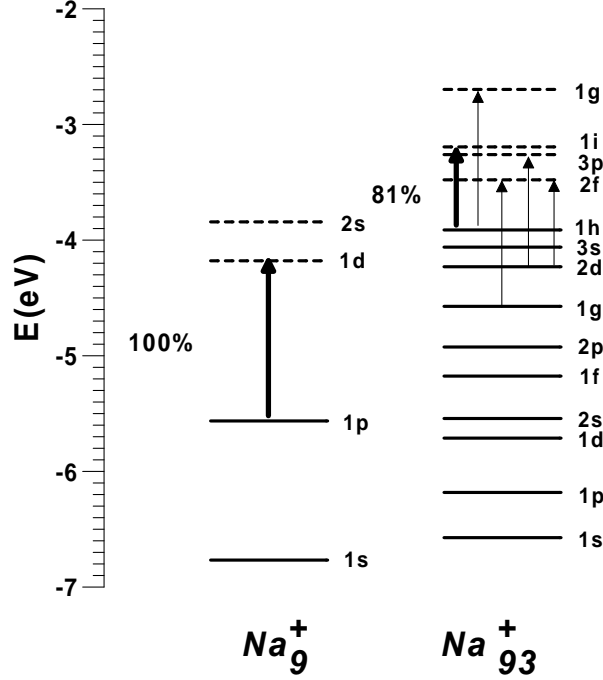


FIG. 9: Single-particle level schemes for the mean field of valence electrons and M2  $1h-1e$  transitions in  $Na_9^+$  and  $Na_{93}^+$ . The levels are labeled by  $\{nl\}$  where  $n$  is the number of radial nodes in the single-electron function and  $l$  is the orbital moment. Transitions corresponding to the dominant twist peak are depicted by bold arrows. Contributions of these transitions to the complete  $B(M2)$  strength are given in %.

of concentration decreases with  $N_e$ . The twist peak exhausts 100%, 80%, and 60% of the total M2 strength in  $Na_9^+$ ,  $Na_{93}^+$ , and  $Na_{1315}^+$ , respectively. As was shown in [5], this peak corresponds to the nodeless twist mode plotted in Fig. 7.

The microscopic nature of the twist peak is exemplified in Fig. 9. It represents the  $n, l \rightarrow n, l + 1$  transition between single-particle levels with the node number  $n = 1$  and *maximal* orbital moments  $l$ . The levels belong to the last occupied and first empty electron quantum shells. As a result, the twist can in principle deliver information about single-particle levels with *maximal* orbital momenta near the Fermi surface.

Calculations [5] show that the twist strength *dominates* over the spin strength already in clusters with  $N_e = 40$ . Starting with  $N_e = 92$ , the orbital contribution becomes overwhelming and demonstrates for  $N_e = 440$  a huge value of  $2 \cdot 10^5 \mu_B^2 \text{\AA}^2 eV$ . As both spin and orbital long-wave M1 responses are forbidden in spherical clusters (their M1-transition matrix elements are proportional to the radial integral  $\int R_{n_1 l_1}(r) R_{n_2 l_2} r^2 dr = \delta_{n_1 l_1, n_2 l_2}$  and thus vanish in the non-diagonal case subject to ortho-normalization requirement), the twist becomes the *strongest* multipole magnetic mode already for clusters of medium size. This emphasizes its fundamental character.

The search for the twist in atomic clusters is a demanding problem. This mode cannot be observed in photoabsorption (only dipole) or two-photon processes (only natural parity). Exploration of twist in atomic nuclei hints that one might try to search this mode in clusters by means of angular resolved electron-energy-loss-spectroscopy (EELS) [23, 47, 48]. Since twist contributes to the transverse form-factor, the back angles of scattered electrons are most suitable.

### III. EXPERIMENTAL ACCESS TO NON-DIPOLE MODES

#### A. General view

As compared with other non-dipole modes, infrared quadrupole states deserve special attention. There are at least two samples, i) free light deformed clusters and ii) oriented silver rods embedded in a matrix, where these modes can be studied experimentally in two-photon processes. The light deformed clusters are especially interesting [7] since their quadrupole modes provide access to the single electron spectra. In turn, the spectra can serve as a sensitive indicator of several cluster properties. It is known that just small clusters demonstrate properties unusual for the bulk and, in this sense, are attractive for both fundamental physics and applications.

Two-photon processes (TPP) are widely used in atomic and molecular physics (for a comprehensive discussion see [52]). Since atomic clusters are similar to molecules, it would be natural to implement the same reactions to clusters. However, applications of TPP to clusters are still very scarce. This can be partly explained by our poor knowledge on non-dipole low-energy electron modes in clusters, and partly by peculiarities of clusters.

In this section we discuss applicability of some traditional TPP methods to clusters with particular emphasis on infrared quadrupole modes. In this connection, some cluster properties essential for TPP should be closely scrutinized. Namely:

i) The dominant decay channel of cluster levels is usually not radiative. The collective states, like the dipole plasmon, mainly decay through Landau fragmentation (dissipation of the collective motion through surrounding  $1eh$  excitations). For non-collective states, the electron-electron collisions and electron-ion coupling are most essential.

ii) *Collective* electron modes in clusters have very short lifetimes. The typical example is the dipole plasmon which represents in medium large clusters with  $N_e \sim 50 - 1000$  a broad ( $\sim 0.5$ - $1$  eV) mode with a life time of 10-20 fs. This is due to a coupling of the collective strength with energetically close  $1eh$  states whose availability increases with increasing cluster size [49, 50]. The mechanism is similar to Landau damping of the plasmon in the bulk electron gas [51]. Its analogue in finite systems is called therefore Landau fragmentation. The short lifetimes hamper application of adiabatic TPP methods as they would require more intense laser irradiation. The intense irradiation results in strong dynamical Stark shifts and undesirable population of high-energy states by second harmonic of the laser pulses. These effects can be detrimental for adiabatic TPP especially if the cluster spectrum is not sufficiently dilute. *Non-collective* electron modes (as low-lying quadrupole  $1eh$  ones) have much longer life times that can approach ps for low temperature and hundreds fs for the room temperature [12, 13]. Unlike molecules, these modes in metal clusters are mainly driven by the mean field similar to the nuclear one. This allows their unambiguous treatment at least in light clusters with 5-20 atoms.

iii) Clusters exhibit a strong shape isomerism. Even beams with size selected clusters usually represent a statistical mix of samples with a multitude of different shapes. This blurs the measured low-energy electron spectra.

The properties i)-iii) are absent in atoms but at least some of them are common for molecules. Thus one may hope that methods of molecular spectroscopy can be applied

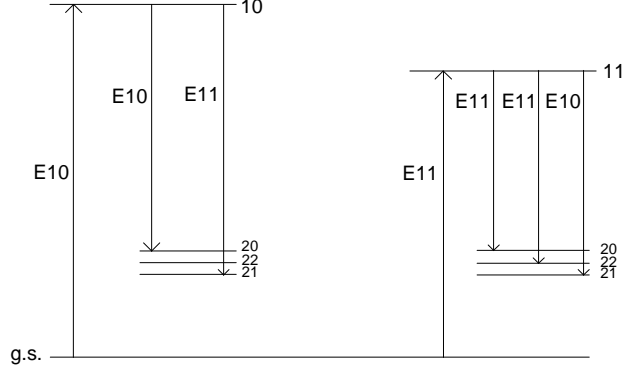


FIG. 10: Two-photon process: scheme of population of infrared quadrupole modes  $\lambda\mu = 20, 21$  and  $22$  via the dipole states with  $\lambda\mu = 10$  (left) and  $11$  (right).

to clusters. It is worth noting that, as compared with molecules, clusters provide new possibilities for investigation of electron modes. The electron spectra in clusters are very diverse (from the collective plasmons to the pure  $1eh$  configurations) and, at the same time, are easily classified and treated in terms of electronic quantum shells.

Light free clusters with 5-20 atoms have dilute spectra, a feature which allows to avoid some of the troubles listed above. Landau fragmentation in such clusters is very weak, the infrared levels are not so broad and their lifetimes are much longer. Most of light clusters have larger isomer energies such that they have one clearly preferred equilibrium shape and many of the energetically close isomeric shapes are similar to the ground state one [22], thus minimizing blurring of the low-energy spectra. Beams of size-selected singly-charged light clusters are readily available. The cluster temperature  $\sim 100$ -200 K could be optimal for our aims. Then the thermal broadening of electron levels is small.

Oriented silver rods embedded into glass [8, 9] represent another interesting sample to be studied in TPP. These clusters are known as commercial polarizers. The polarization is provided by the property of the  $\lambda\mu = 10$  branch of the dipole plasmon to absorb only the light aligned along the symmetry axis of the cluster. Because of the big axis ratio, the rods represent an example of atomic clusters with an extreme deformation. These heavy clusters can be studied in Raman scattering [10].

Following the general TPP scheme presented in Fig. 10, the target quadrupole level is populated via an intermediate dipole state by two (absorption and emission) dipole transitions. Both the collective dipole plasmon and non-collective  $1eh$  configurations can serve as

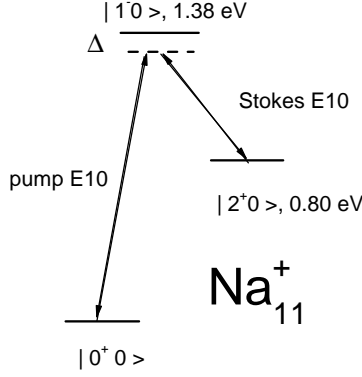


FIG. 11: TPP population transfer from the ground state  $|0^+0\rangle$  to the quadrupole state  $|2^+0\rangle$  via the  $1eh$  dipole state  $|1^-0\rangle$  in  $\text{Na}_{11}^+$ . The detuning from the dipole state is  $\Delta \sim 0.14$  eV.

intermediate states. The TPP via the dipole plasmon, with its broad and smoothed structure and ultra-fast decay through Landau damping, reminds the population transfer via continuum. The TPP via non-collective  $1eh$  dipole states is more transparent and represents the typical population transfer process in tree-bound-state  $\Lambda$ -systems.

As is shown in Fig. 10, there are possible TPP paths via dipole states with  $\lambda\mu = 10$  and 11. These states could be, for instance, branches of the dipole plasmon, separated by the deformation splitting. In the first case, the population of  $\lambda\mu = 22$  mode is forbidden and only 20 and 21 modes can be targeted. This provides some selection when carrying out TPP experiments.

For a crude analysis of TPP in clusters, one may use the rotating wave approximation (RWA) that allows to discard the fast laser frequencies and treat the problem with the much lower Rabi frequencies only. Fig. 11 for  $\text{Na}_{11}^+$  shows a typical electron  $\Lambda$ -system and hence the scale of the laser frequencies corresponding to photoabsorption (pump) and photoemission (Stokes) processes. Following our calculations, even for laser pulses with intensity  $I \sim 10^{10} \text{ W/cm}^2$ , Rabi frequencies in light deformed sodium clusters lie in the interval  $10^{-1} - 10^{-2}$  eV. Obviously, they are much less than the carrier (laser) frequencies and thus fulfill the main RWA requirement. Besides, because of the pretty long life-time of the target non-collective quadrupole states, one may operate with long laser pulses covering many Rabi cycles. Hence we match the second RWA requirement.

In the next subsections, we will consider some widespread two-photon processes (Raman Scattering (RS), Stimulated Emission Pumping (SEP), and Stimulated Raman Adiabatic

Passage (STIRAP)) and estimate their ability to observe infrared quadrupole modes.

## B. Raman scattering

RS is one of the simplest two-photon processes where a dipole laser-induced transition to an intermediate electronic level (real or virtual) is followed by the dipole spontaneous fluorescence to low-energy levels.

RS measurements of electron infrared modes in clusters are yet very rare. For instance, the quadrupole infrared modes were observed in heavy silver clusters embedded into amorphous silica films [31]. The dipole plasmon was used as a resonant intermediate state. In the recent experiment of this group with another sample (oriented silver rods embedded into glass), the infrared electron quadrupole mode, probably  $\lambda\mu = 20$ , was detected [10]. These observations show that the dipole plasmon can be used as intermediate state for TPP in spite of its extremely short lifetime. This is the encouraging message for TPP implementation to clusters.

RS generally assumes that the coupling between the intermediate dipole and target quadrupole states, from one side, and the coupling between the intermediate and ground states, from the other side, are of the same order of magnitude. Only then the final state is successfully populated. This means that the absorption and emission dipole matrix elements should be of the same scale. Experiments of E. Duval [10, 31] show that this is indeed the case for heavy clusters. In light deformed clusters the situation is more complicated. Our calculations [7] for  $\text{Na}_7^+$ ,  $\text{Na}_{11}^+$  and  $\text{Na}_{15}^+$  revealed that the absorption and emission dipole matrix elements lie mainly in the interval 2-10  $ea_0$  (atomic units) and thus are basically similar. This means that infrared quadrupole modes in light deformed clusters have a chance to be observed in the resonant RS running via the dipole plasmon. However, we have also found a few exceptions when the Stokes couplings are strongly suppressed due to destructive interference effects (see discussion in [7]). The particular example is oblate  $\text{Na}_7^+$  where only the path via the  $\lambda\mu = 11$  branch of dipole plasmon results in a strong TPP while the alternative path via the  $\lambda\mu = 10$  branch is about completely suppressed. Such considerable variations for different paths are not surprising for small clusters where electronic spectra and transition rates are very specific and can appreciably change from one sample to another. In clusters with suppressed dipole couplings, the RS is not effective. Besides, the RS

has a general drawback that its photoemission step is fully dictated by competition between different decay channels of the intermediate state. As a result, the spontaneous fluorescence to the target state and hence the RS efficiency is typically rather low. To overcome this trouble, we should consider methods with *stimulated* emission into the target level.

### C. Stimulated emission pumping

The stimulated emission pumping (SEP) enjoys widespread application for atoms and molecules and seems to be very promising for population of infrared quadrupole states in clusters. Unlike RS, this method exploits two lasers, pump and Stokes (or dump) [53, 56]. The pump pulse is responsible for the first photoabsorption step. The Stokes pulse couples the intermediate state to the target one. The pulses can be simultaneous or sequential. If the difference between the pump and Stokes frequencies is in resonance with the frequency of the target state, then the Stokes radiation stimulates emission to this state.

One should distinguish SEP with incoherent and coherent irradiation. If incoherent light sources are used, then, even in the best case of the saturated process and coincident pump and Stokes pulses, the maximal SEP efficiency achieves only one-third of the complete population [56]. In practice, the transfer efficiency does not exceed 10%. However, even this value is enough for many spectroscopic studies.

A much better population can be achieved for coherent laser irradiation. If the pump and Stokes pulses coincide, then under certain requirements (given in the next subsection) we can even gain the fully adiabatic process (with still not complete population transfer as compared with STIRAP [57]). In this subsection, we consider the coherent SEP with an appreciable detuning (often called as off-resonant stimulated Raman). This process promises a simple, robust and efficient population scheme.

We present below our TDLDA results for SEP in  $\text{Na}_{11}^+$ . The calculations explore the time evolution of the initial single-electron states. All the possible channels including photoionization (through absorbing boundary conditions) are taken into account. The ions are considered in soft jellium approximation at fixed deformation. The details of the method are described elsewhere [12, 13]. The parameters of the Stokes and pump pulses are given the panel (c). Their frequencies maintain the two-photon resonance with the target state:  $\omega_p - \omega_s = \omega_{2+0}$  and are detuned somewhat below the intermediate dipole state,



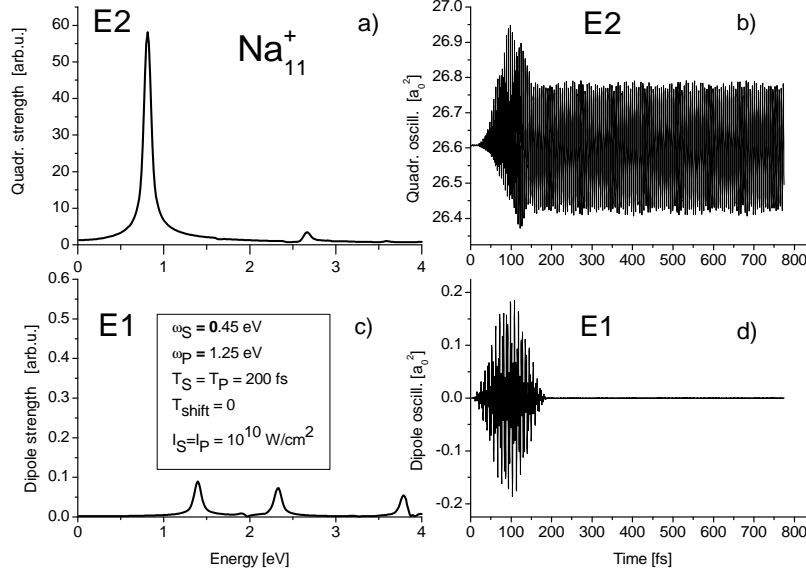


FIG. 12: Off-resonant SEP population transfer from the ground state to the quadrupole state  $|2^+0\rangle$  via the  $1eh$  dipole state  $|1^-0\rangle$  in  $\text{Na}_{11}^+$ . The left plots exhibit (in arbitrary units) strengths of quadrupole (a) and dipole (c) modes as a function of their energy. The right plots depict (in atomic units) time evolutions of the overwhelming quadrupole mode with  $\omega_{2+}=0.80$  eV (b) and dipole oscillations (d). Specifically, the oscillations of the quadrupole and dipole moments are presented. The parameters of the Stokes (s) and pump (p) pulses (frequency  $\omega$ , duration  $T$  and intensity  $I$ ) are given in the panel (c). The pulse profile is the squared cosine.

$\Delta = (\omega_{1-} - \omega_{0+}) - \omega_p = (\omega_{1-} - \omega_{2+}) - \omega_s = 0.14$  eV, so as to minimize its population. It is worth noting that an appreciable detuning is crucial as the dipole couplings in clusters are rather strong. This is the only way to suppress undesirable population of other dipole and quadrupole states and thus to enhance the population of the target state.

In Fig. 12, the TPP via the isolated non-collective dipole level at 1.38 eV is considered (the actual  $\Lambda$ -system is presented in Fig. 11). The quadrupole ( $\lambda = 2$ ) and dipole ( $\lambda = 1$ ) strengths  $\sigma_{E\lambda}(\omega) = \sum_j \langle j | r^\lambda Y_{\lambda\mu} | 0 \rangle^2 \delta(\omega_j - \omega)$  versus their excitation energy are depicted in the left panels. Panel (a) demonstrates the strong quadrupole excitation at 0.80 eV. Because of the considerable detuning, all other quadrupole and dipole modes are pretty small. The right panels (b) and (d) show that, while dipole oscillations survive only during the irradiation time  $\sim 200$  fs, the quadrupole oscillations around the static values  $Q_2 = 26.6 a_0^2$  ( $a_0$  is the

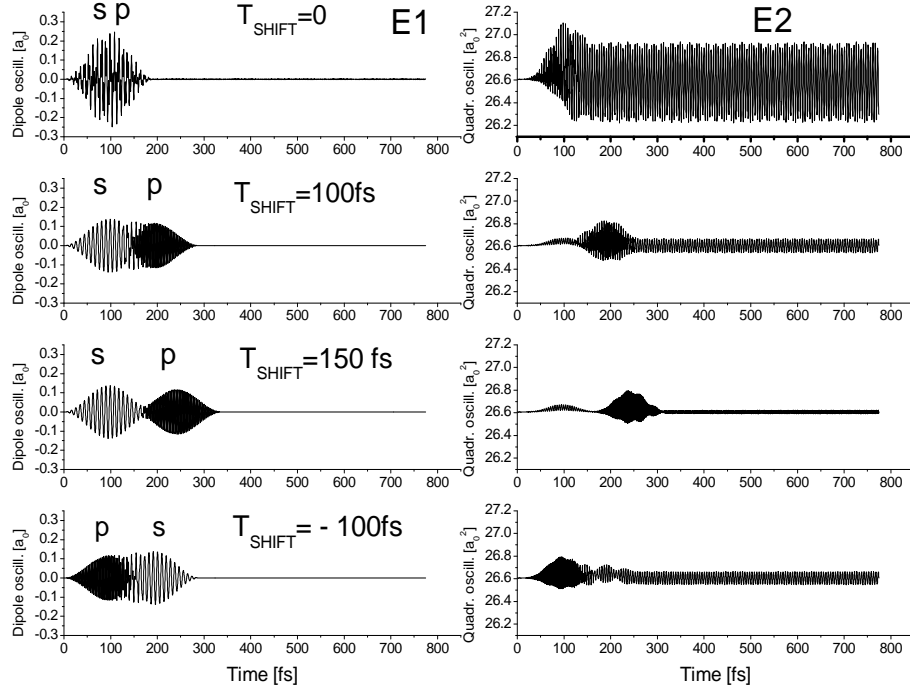


FIG. 13: Time evolution of dipole and quadrupole oscillations for different pulse shifts (sequences) in  $\text{Na}_{11}^+$ . The values of the shifts between the Stokes (s) and pump (p) pulses are depicted at the left plots. The pulse parameters are the same as in Fig. 12 for exception of  $I_s = 3.3 \cdot 10^{10} \text{ W/cm}^2$ .

Bohr atomic unit) are *very enduring*. There is no any attenuation until 800 fs. Our study shows that the lifetime of this mode is even longer and achieves at least a few ps. Because of the dilute spectrum, decay of this mode via the electron-electron coupling is negligible. Only the coupling with the ions remains but it is not taken into account in these calculations. The electron-ion coupling should limit lifetime of the mode by a few hundred fs at a room temperature and by a few ps at a minimal temperature  $\sim 10$  K. The latter case corresponds to our analysis.

The calculations show that the enduring quadrupole mode is also produced in TPP running through the dipole plasmon. In this case, the mode is even several times stronger. The pulses with the frequencies  $\omega_P = 2.04$  eV and  $\omega_P = 1.24$  eV and the same intensities and durations as in Fig. 12 were used. The pulses were appreciably detuned from the dipole plasmon so as to weaken the competing channels (compare  $\omega_P = 2.04$  eV with the dipole plasmon in  $\text{Na}_{11}^+$  depicted in Fig. 1). It is remarkable that the dipole plasmon can be used as

the effective mediator in spite of its extremely short lifetime. The key point is the detuning that prevents the population of the plasmon and thus the leaking from it. Using the dipole plasmon as the intermediate state has the additional advantage of dealing with the well known structure rather than with still poorly known low-energy dipole states.

Fig. 13 demonstrates the dependence of the quadrupole signal on the sequence of the pump and Stokes pulses. It seen that the quadrupole mode is maximal at simultaneous pulses. This is the typical SEP case. The process is rather robust to changes of pulse characteristics. The calculations show that variations by several times in pulse durations and intensities still maintain the stable and distinctive SEP (though with the rescaled mode amplitude). Of course, any change in the pulse intensities should be compensated by the corresponding modification of the detuning.

It is a non-trivial problem to detect the quadrupole mode populated in SEP. In principle, this could be done by using the probe laser with supplemented PES (photoelectron spectra) spectroscopy. The probe laser should be intense enough to result in measurable PES and its frequency should be large to map the single-electron states in the cluster and thus provide the complete PES [58]. In  $\text{Na}_{11}^+$ , it could be  $\omega_{probe} \sim 7 - 8$  eV. The probe pulse should follow the pump one with a considerable delay so as to avoid overlapping with the latter and map only the endurant quadrupole mode. Due to the Raman coupling of the single-electron PES with the quadrupole oscillation, every PES should acquire left and right satellites with the relative frequencies coinciding with  $\omega_{2+}$ . Hence we get the frequency of the quadrupole state. The strategy is to keep the fixed pump frequency with a reasonable detuning bellow the intermediate dipole state and scan the Stokes frequency. When we get the resonance satellites  $\omega_P - \omega_S = \omega_{2+}$ , then the endurant quadrupole mode has to be produced and detected. It may happen that the Stokes frequency maps a dipole state. In that case the endurant dipole oscillation are accompanied by a subsequent considerable increase of photoemission yield together with the appearance of dipole satellites. Such cases can be easily separated from the case of interest, population of the quadrupole mode, since the latter is not associated with a significant resonant increase in photoemission yield but only by the satellites signature alone.

The SEP experiments usually need three lasers: pump, Stokes and probe. However, one may propose the simpler recipe with implementation of only pump and probe lasers. Such scheme assumes the combination of the direct two-photon excitation of the quadrupole

state and PES techniques. Specifically, the intense pump laser should scan until its two photons excite the quadrupole state. Then the delayed probe laser is applied in the manner described above to detect the population. The calculations show that this simple method is quite effective and robust.

#### D. STIRAP

The STIRAP method [54, 55, 56] promises up to 100% population transfer from the initial to the target level. This high efficiency is achieved by the *coherent adiabatic* character of the process and the principle possibility to avoid any leaking from the intermediate levels. Like SEP, STIRAP also implements pump and Stokes lasers providing the couplings  $|0\rangle \rightarrow -|1\rangle$  and  $|1\rangle \rightarrow -|2\rangle$ , where  $|0\rangle$ ,  $|1\rangle$  and  $|2\rangle$  are initial ground state, intermediate dipole state and target quadrupole states, respectively. However, STIRAP is much more involved. Its main requirements are:

- i) *Two-resonance condition*  $\omega_P - \omega_S = \omega_2 - \omega_0$  with a possible detuning  $\Delta = (\omega_1 - \omega_0) - \omega_P = (\omega_1 - \omega_2) - \omega_S$  from the intermediate state frequency.
- ii) *Counterintuitive sequence* of partly overlapped pulses when the Stokes pulse comes before the pump one.
- iii) *Adiabatic passage* of the state vector from the initial to the target state. The adiabaticity condition (for the detuning  $\Delta=0$ ) has the form

$$\Omega\Delta\tau \gg 1 \tag{16}$$

where  $\Omega = \sqrt{\Omega_p^2 + \Omega_s^2}$  is the average of the pump and Stokes Rabi frequencies and  $\Delta\tau$  is the overlapping time of the pulses (duration of the evolution process).

Under these requirements, one of the adiabatic time-dependent eigen-functions of the system becomes a superposition of the initial and target bare states only:  $|b_0(t)\rangle = c_0(t)|0\rangle + c_2(t)|2\rangle$ . This is so called *dark* state. It is reduced to  $|0\rangle$  at the beginning of the adiabatic evolution and to  $|2\rangle$  at the end. Hence, the system finally finds itself in the target state. The intermediate state  $|1\rangle$  is not involved in  $|b_0(t)\rangle$  and thus is not populated at any time. Thus any leaking in the population is avoided and the transfer is complete. The main point is to evolve the system adiabatically, keeping it all the time in the state  $|b_0(t)\rangle$ . STIRAP is well known in atomic and molecular spectroscopy. It is rather insensitive to precise pulse

characteristics. Both continuous and pulse lasers can be implemented.

Let's now examine the STIRAP requirements for the case of infrared quadrupole modes in atomic clusters

*Two-resonance condition.* The better fulfilled this condition, the less mixing of the dark adiabatic state  $|b_0(t)\rangle$  with the state  $|1\rangle$  and thus more robust the STIRAP. In practice, this condition is perturbed by the detrimental dynamical (time dependent) Stark shifts of the electron levels [56]

$$S_s(t) = -\frac{\Omega_s^2(t)}{4\Delta}, \quad S_p(t) = -\frac{\Omega_p^2(t)}{4\Delta}. \quad (17)$$

Too strong Stark shifts perturb the STIRAP balance and destroy the adiabatic process. The Rabi frequency reads [54, 56]

$$\Omega = \frac{|d|}{\hbar} \sqrt{\frac{2I}{c\epsilon_0}} \simeq 2.20 \cdot 10^8 |d[ea_0]| \sqrt{I[\frac{W}{cm^2}]} s^{-1}, \quad (18)$$

where  $d$  is the dipole coupling matrix element in atomic units,  $I$  is the laser intensity in  $W/cm^2$ ,  $c$  is the light speed,  $\epsilon_0$  is the vacuum dielectric constant. It is seen that  $\Omega \sim \sqrt{I}$  and thus  $S \sim I$ . So, the smaller the laser intensity, the weaker the Stark shift. However, the intensity cannot be too small because of the adiabaticity condition (16). The detuning  $\Delta$  also has the upper limit established by the Rabi frequency  $\Omega$ .

Following our calculations, the coupling dipole matrix element in light clusters is  $d \sim 1 - 5 ea_0$ . If to put the laser intensity  $I = 10^{10} W/cm^2$ , then Eq. (18) estimates the peak Rabi frequency as  $\Omega \sim 0.02 - 0.1$  fs or  $\hbar\Omega \sim 0.01 - 0.07$  eV. These values are less than the detuning  $\Delta=0.136$  eV used for the SEP analysis in the previous subsection. Thus the SEP was obtained at the tail of the dipole coupling between the states of the  $\Lambda$ -system. Under the given detuning and laser intensity, the Stokes shift is  $S \sim 0.0004 - 0.01$  eV which is still a bearable value.

*Counterintuitive order of pump and Stokes pulses.* The order when Stokes pulse precedes the pump one is crucial for the complete population since only then the state vector can be fully projected into the dark adiabatic state  $|b_0(t)\rangle$  [54, 55]. Stokes and pump pulses must overlap and the overlapping time  $\Delta\tau$  determines the duration of the adiabatic evolution.

The  $\Delta\tau$  should not be longer than the lifetimes of the initial and target states while the lifetime of the intermediate state does not matter if this state is not populated. So, the ultra-short lifetime of the dipole plasmon (10-20 fs) is not the problem for the ideal STIRAP. Even under some leaking from the plasmon (and thus the modest coupling of the dark state

$|b_0(t) >$  with  $|1 >$ ) STIRAP is still possible. This is partly confirmed by recent experiment [59] where STIRAP was induced via continuum. Even in this extreme case with ultra-fast decay channels and considerable leaking, a clear STIRAP population transfer was obtained (though with low efficiency  $\sim 6\%$ ).

When STIRAP runs via an isolated non-collective dipole state, like that with  $\omega = 0.80$  eV in  $\text{Na}_{11}^+$ , then the situation is much simpler. Following the estimations for the lifetimes of  $1eh$  state, the value of  $\Delta\tau$  should not exceed a few hundreds fs at room temperature and a few ps at low temperature.

It should be emphasized that the maximal population transfer at the counterintuitive order of pump and Stokes pulses is the main signature of STIRAP. Just this feature allows finally to judge if we deal with STIRAP or other processes like SEP.

*Adiabatic passage.* This requirement is crucial for STIRAP. Only adiabatic evolution can ensure the steady complete populations. The adiabaticity condition is given by Eq. (16). If we put, following the above estimations,  $\Omega \sim 0.02 - 0.1 fs$  and  $\Delta\tau \sim 300 fs$ , then it is easy to see that the adiabaticity condition is fulfilled:  $\Omega\Delta\tau \sim 6 - 30 \gg 1$ . However, the situation is not so simple since Eq. (16) does not take into account the detuning that effectively weakens the Rabi frequency. In practice, we should use an appreciable detuning to minimize the competing channels. But then  $\Omega$  is considerably decreased and the adiabatic condition is violated. This becomes a real hindrance when the electron spectrum is not dilute enough.

It worth noting that the adiabaticity condition (16) can be considerably relaxed. Indeed, it was derived for *one* intermediate level. But the realistic spectrum of the dipole plasmon consists of a broad structure consisting from a sequence of dipole levels (see Fig. 1). In this case, the STIRAP adiabatic condition should be revised. The realistic case is more complicated but, at the same time, opens new possibilities for STIRAP. In particular, one may be allowed to loose the adiabatic STIRAP condition and thus the requirements for the laser intensity.

A general case of  $N$  intermediate states, each with its own coupling and detuning was studied in [60]. It was shown that the trapped adiabatic state  $|b_0(t) >$  can be created only when the ratio between each pump coupling and the respective Stokes coupling is the same for all intermediate states. Following our calculations, this condition is unrealistic for atomic clusters. However, softer alternative adiabatic requirements can be formulated. In particular, in the general case of arbitrary couplings, one may tune the pump and Stokes

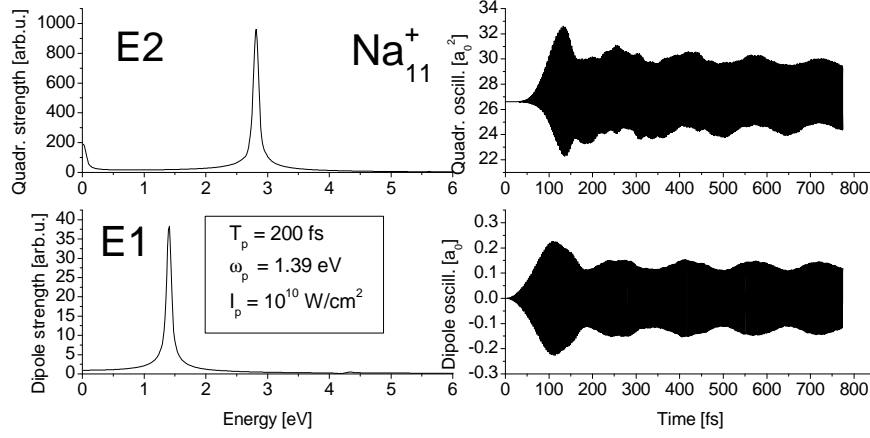


FIG. 14: Simultaneous resonant excitation of the dipole state and quadrupole plasmon in  $\text{Na}_{11}^+$  by the first and second pump harmonics, respectively. The up and middle left plots exhibit strengths of the quadrupole and dipole modes as a function of their energy. The right plots depict time evolutions of these modes.

lasers just below all intermediate states and thus form so called adiabatic-transfer state which also results in a high, although not complete, population of the target level. Unlike  $|b_0(t)\rangle$ , the adiabatic-transfer state can have admixture from the intermediate states during the evolution period  $\Delta\tau$  and so some population leaking is unavoidable. Nevertheless, we have here a solid adiabatic transfer with a high population of the target state. Just this method is implemented in our calculations while using the dipole plasmon as the intermediate TPP state.

Altogether, the arguments and estimations presented above show that STIRAP is possible in clusters. However, it is not so trivial to find the optimal parameters of the process and get STIRAP in realistic TDLDA calculations. Serious problems arise in connection with dipole and quadrupole plasmons which reside in the energy region 2 - 4 eV and thus are always covered by multiphoton excitations of the pump and Stokes pulses. Hence there arises a considerable undesirable population leaking. Especially strong coupling with the

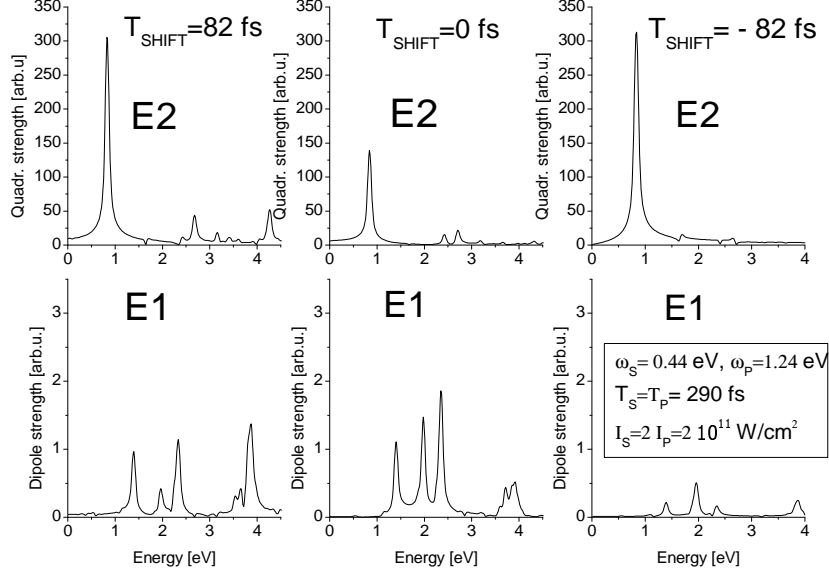


FIG. 15: Population transfer from the ground state to the quadrupole state  $|2^+0\rangle$  via the  $1eh$  dipole state  $|1^-0\rangle$  in  $\text{Na}_{11}^+$ . The up and low panels represent the quadrupole and dipole strengths at different delays (shifts) of the pump pulse versus the Stokes one: 82 fs (counterintuitive STIRAP pulse sequence), 0 fs (coinciding pulses), -82 fs (intuitive pulse sequence). The parameters of the Stokes (s) and pump (p) pulses (frequency  $\omega$ , duration  $T$  and intensity  $I$ ) are given in the low-right panel.

quadrupole plasmon takes place when the pump or Stokes frequencies are in resonance with some dipole state. The example of such process is exhibited in Fig. 14 where the resonant excitation of the dipole state at 1.38 eV leads to a huge population of the quadrupole plasmon. This means that we should avoid the resonance cases by imposing appreciable detuning. But, as was mentioned above, this will effectively weaken the Rabi frequencies. Then, to keep the requirement (16), one should use longer pulses. This is quite possible at low temperatures when the lifetimes of the states can reach a few ps. In this case, we even have the freedom to decrease the laser intensity with the aim to minimize the Stark shifts.

The proper choice of the pulse parameters allows to produce a STIRAP-like process in clusters even at high laser intensity. A successful example is presented in Fig. 15. A large detuning of  $\Delta = 0.15$  eV is here combined with a high pulse intensity of  $I \sim 10^{11} \text{ W/cm}^2$ . This particular choice allows to minimize the impact of the quadrupole and



dipole plasmons and, at the same time, to keep the adiabaticity condition. Fig. 15 shows that the counterintuitive pulse sequence provides the stronger strength of the quadrupole mode than the coinciding pulses. In terms of the population, this could be the unequivocal signature of the STIRAP. As is seen from the figure, the intuitive pulse sequence also results in the same quadrupole strength. It looks like this TPP embraces not only the typical STIRAP branch corresponding to the dark state  $|b_0\rangle$  but also the branch from the dark state  $|b_+\rangle$ . The latter takes place because of the large detuning below the intermediate dipole state. Following [61], an appreciable detuning below or above the intermediate state results in the additional dark dressed state  $|b_+\rangle$  or  $|b_-\rangle$ , respectively.

Though the process in Fig. 15 looks like STIRAP, its STIRAP nature still should be proved. The point is that the strength exhibited in Fig. 15 does not correspond to the population (squared amplitude of the target state) but rather to the coherence (product of amplitudes of initial and target states). Hence, the maxima of the strength at non-zero pulse shifts still do not mean that the similar maxima take place for the population of the target state. Our TDLDA model does not allow to estimate properly the population. However, this can be done within the Rotating Wave Approximation for 3-level  $\Lambda$ -system [56]. Following these estimations, we have found that the TPP in the example above has the maximal population at coinciding pulses and thus is not STIRAP. For getting the STIRAP we need more intense laser pulses and maybe another value of the detuning. One may get other, and more favorable, options in clusters by a more suitable choice of the process parameters, set to worked out. In any case, the example in Fig. 15 hints the principle possibility of STIRAP in atomic clusters. The experimental detection of the STIRAP population can be done by the same methods as in SEP.

The application of STIRAP to clusters seems to be generally feasible. At the same time, this process is more demanding to realize than SEP. It requires further studies within realistic TDLDA models to look for the most effective process configurations. STIRAP can hardly be more practicable than SEP in population and detection of infrared quadrupole modes in clusters. However, one may try to implement STIRAP to get more transfer efficiency in particular cases. Besides, STIRAP running via the dipole plasmon can be interesting for theory of adiabatic TPP as such. Indeed, the intermediate state like the dipole plasmon does not exist in atoms and molecules and so was not yet investigated. Perhaps, this intermediate state will offer new options for STIRAP and extend our knowledge about this intriguing TPP.

## IV. CONCLUSION

Non-dipole infrared electron modes in atomic clusters (electric quadrupole (E2), magnetic dipole scissors (M1) and magnetic quadrupole twist (M2)) were analyzed theoretically using as tool the time-dependent local-density approximation (TDLDA). The collective and non-collective nature of these modes as well as their connection with the basic cluster properties (single electron spectra, orbital magnetism) were analyzed in detail. Free light deformed sodium clusters and embedded oriented silver rods were considered as the most promising samples. The possible routes of experimental observation of infrared quadrupole modes in two-photon processes (Raman scattering, stimulated emission pumping (SEP) and stimulated Raman adiabatic passage (STIRAP)) were scrutinized. Following our analysis, the combination of SEP and PES techniques provides probably the most simple and robust way to populate and detect the infrared quadrupole states in free light deformed clusters. As a complementary method, a technique using direct two-photon excitation was also considered. The Raman scattering seems to be optimal for large clusters, especially embedded oriented silver rods. The calculations encourage applicability of STIRAP to clusters. However, this intriguing but demanding method still needs further realistic TDLDA studies. Smaller clusters as, e.g.,  $\text{Na}_7^+$  are the most promising candidates.

We hope that our study will stimulate investigation of non-dipole electron modes in clusters by means of TPP experimental methods. This would provide a deeper understanding both clusters properties and peculiarities of different TPP schemes.

## Acknowledgement

V.O.N. thanks Professors K. Bergmann, E. Duval and J.-M. Rost and Junior Professor T. Halfmann for useful discussions. The work was partly supported by the Bundesministerium Bildung und Forschung (project No. 06ER124), the Visitors Program of Max Planck Institute for the Physics of Complex Systems (Dresden, Germany) and Heisenberg-Landau program (Germany - BLTP JINR).

- 
- [1] V.O. Nesterenko, W. Kleinig, and F.F. de Souza Cruz, in Proc. of Intern. Workshop "Collective excitations in Fermi and Bose Systems", Serra Negra, San Paulo, Brazil, 1998 edited by C.A.

- Bertulani, L.F. Canto and M.S. Hussein (World Scientific, Singapore, 1999), p. 205-224.
- [2] E. Lipparini and S. Stringari, Phys. Rev. Lett. **63**, 570 (1989).
  - [3] E. Lipparini and S. Stringari, Z. Phys. D **18**, 193 (1991).
  - [4] V.O. Nesterenko, W. Kleinig, F.F. de Souza Cruz and N. Lo Iudice, Phys. Rev. Lett. **83**, 57 (1999).
  - [5] V.O. Nesterenko, J.R. Marinelli, F.F. de Souza Cruz, W. Kleinig and P.-G. Reinhard, Phys. Rev. Lett., **85**, 3141 (2000).
  - [6] V.O. Nesterenko, W. Kleinig, P.-G. Reinhard, N. Lo Iudice, F.F. de Souza Cruz, and J.R. Marinelli, Eur. Phys. J. D **27**, 43 (2003).
  - [7] V.O. Nesterenko, P.-G. Reinhard, W. Kleinig, and D.S. Dolci, Phys. Rev. A. **70**,023205 (2004).
  - [8] A.Berger, J. Non-Cryst. Solids **163**, 185 (1993).
  - [9] S. Polizzi, P. Riello, G. Fagherazzi, and N.F. Borelli, J. Non-Cryst. Solids **232-234**, 147 (1998).
  - [10] E. Duval, private communication.
  - [11] W. Kleinig, V.O. Nesterenko, and P.-G. Reinhard, Ann. Phys. (NY) **297**, 1 (2002).
  - [12] F. Calvayrac, P.-G. Reinhard, E. Suraud, and C.A. Ullrich, Phys. Rep. **337**, 493 (2000).
  - [13] P.-G. Reinhard and E. Suraud, *Introduction to Cluster Dynamics*, (Wiley-VCH, Berlin, 2003).
  - [14] W.A. de Heer, Rev. Mod. Phys. **65**, 611 (1993).
  - [15] M. Brack, Rev. Mod. Phys. **65**, 677 (1993).
  - [16] K. Clemenger, Phys. Rev. B **32**, 1359 (1985).
  - [17] O. Gunnarson and B.I. Lundqvist, Phys. Rev. B **13**, 4274 (1976).
  - [18] B. Montag, Th. Hirschmann, J. Meyer, P.-G. Reinhard, and M. Brack, Phys. Rev. B **52**, 4775 (1995).
  - [19] W. Kleinig, V.O. Nesterenko, P.-G. Reinhard, and Ll. Serra, Eur. Phys. J. D **4**, 343 (1998).
  - [20] V.O. Nesterenko, W. Kleinig, and P.-G. Reinhard, Eur. Phys. J. D **19**, 57 (2002).
  - [21] M. Schmidt and H. Haberland, Eur. Phys. J. D **6**, 109 (1999).
  - [22] S. Kümmel, M. Brack, and P.-G. Reinhard, Phys. Rev. B **62**, 7602 (2000).
  - [23] L. G. Gerchikov, A. N. Ipatov, A. V. Solov'ev, and W. Greiner, J. Phys. B **31**, 3065 (1998).
  - [24] G. Wrigge, M.A. Hoffmann and B. v. Issendorff, Phys. Rev. A **65** 063201 (2002).
  - [25] N. Lo Iudice and F. Palumbo, Phys. Rev. Lett. **41**, 1532 (1978).
  - [26] D. Bohle *et al*, Phys. Lett. **137B**, 27 (1984).
  - [27] Ll. Serra, A.Puente, and E. Lipparini, Phys. Rev. B **20**, R13966 (1999).

- [28] A. Minguzzi and M.P. Tosi, arXiv:cond-mat/0005098, 2000.
- [29] D. Guéri and S. Stringari, Phys. Rev. Lett. **83**, 4452 (1999).
- [30] O.M. Maragó, S.A. Hopkins, J. Arlt, E. Hodby, G. Hechenblaikner, and C.J. Foot, Phys. Rev. Lett. **84**, 2056 (2000).
- [31] H. Portales, E. Duval, L. Saviot, M. Fujii, M. Sumitomo, and S. Hayashi, Phys. Rev. B **63**, 233402 (2001).
- [32] P.-G. Reinhard, V.O. Nesterenko, E. Suraud, S. El Gammal, and W. Kleinig, Phys. Rev. A **66**, 013206 (2002).
- [33] L.D. Landau, Z.Phys. **64**, 629 (1930).
- [34] A.I. Buzdin, O.V. Dolgov, and Yu. E. Lozovik, Phys. Lett. A **100**, 261 (1984).
- [35] V. Kresin, Phys. Rev. B **38**, 3741 (1988).
- [36] J.M. van Ruitenbeek and D.A. van Leewen, Phys. Rev. Lett. **67**, 640 (1991).
- [37] S. Frauendorf, V.M. Kolomietz, A.G. Magner, and A.I. Sanzhur, Phys. Rev. B **58**, 5622 (1998).
- [38] S. Frauendorf, V.V. Pashkevich, and S.M. Reimann, Surf. Rev. Lett. **3**, 441 (1996).
- [39] C. Binns, Surf. Sci. Rep. **44**, 1 (2001).
- [40] H. Lamb, Proc. London Math. Soc. **13**, 187 (1882).
- [41] G. Holzward and G. Ekardt, Z. Phys. A **283**, 1532 (1978); *Nucl. Phys.* A **325**, 1 (1979).
- [42] B. Schwesinger, Phys. Rev. C **29**, 1475 (1984).
- [43] S. I. Bastrukov and I.V. Molodtsova, Phys. Part. Nucl. **26**, 180 (1995); S. I. Bastrukov, Phys. Rev. E **49**, 3166 (1994).
- [44] P. von Neumann-Cosel et al, Phys. Rev. Lett. **82**, 1105 (1999).
- [45] X. Viñas, R. Roth, P. Schuck, and J. Wambach, Phys. Rev. A **64**, 055601 (2001).
- [46] J. M. Blatt and V. F. Weisskopf, *Theoretical Nuclear Physics* (John Wiley & Sons, Inc., New York, 1952).
- [47] T.L. Ferrell and P.M. Echenique, Phys. Rev. Lett. **55**, 1526 (1985).
- [48] W. Ekardt, Phys. Rev. B **32**, 1961 (1985); **33**, 8803 (1986); **36**, 4483 (1987)
- [49] P.-G. Reinhard, O. Genzken, M. Brack, Ann. Phys. (Leipzig) **5**, 576 (1996)
- [50] J. Babst, P.-G. Reinhard, Z. Phys. D **42**, 209 (1997)
- [51] E.M. Lifschitz, L.P. Pitajewski, *Lehrbuch der Theoretischen Physik*, Vol. X, *Physikalische Kinetik*, Mir, Moscow 1988
- [52] *Atomic and Molecular Beam Methods*, ed. G. Scoles, (Oxford Univ. Press, Oxford, 1988).

- [53] *Molecular dynamics and spectroscopy by stimulated emission pumping*, ed. H.-L. Dai and R.W. Field (Advanced series in physical chemistry, **4**, World Scientific, Singapore, 1999).
- [54] K. Bergmann and B.W. Shore, in *Molecular dynamics and spectroscopy by stimulated emission pumping*, ed. H.-L. Dai and R.W. Field (Advanced series in physical chemistry, **4**, World Scientific, Singapore, 1999), Chapter 9, p. 319.
- [55] K. Bergmann, H. Theuer, and B.W. Shore, Rev. Mod. Phys. **70**, 1003 (1998).
- [56] N.V. Vitanov, M. Fleischhauer, B.W. Shore and K. Bergmann, Adv. Atom. Mol. Opt. Phys., **46** 55 (2001).
- [57] N.V. Vitanov, J. Phys. B**31**, 709 (1998).
- [58] A. Pohl, P.-G. Reinhard, E. Suraud, Phys. Rev. Lett. **84**, 5090 (2000).
- [59] T. Peters, L.P. Yatsenko, and Th. Halfman, private communication.
- [60] N.V. Vitanov and S. Stenholm, Phys. Rev. A **60**, 3820 (1999).
- [61] U. Gaubatz, P. Rudecki, S. Schiemann, and K. Bergmann, J. Chem. Phys. **92**, 5363 (1990).